PAPER • OPEN ACCESS

Performance scaling and trade-offs for collective motor-driven transport

To cite this article: Matthew P Leighton and David A Sivak 2022 *New J. Phys.* **24** 013009

New Journal of Physics
The open access journal at the forefront of physics

Deutsche Physikalische Gesellschaft DPG
IOP Institute of Physics

Published in partnership with: Deutsche Physikalische Gesellschaft and the Institute of Physics

OPEN ACCESS

RECEIVED
31 August 2021

REVISED
16 November 2021

ACCEPTED FOR PUBLICATION
26 November 2021

PUBLISHED
4 January 2022

PAPER

Performance scaling and trade-offs for collective motor-driven transport

Matthew P Leighton and David A Sivak*

Department of Physics, Simon Fraser University, Burnaby, British Columbia, V5A 1S6, Canada
* Author to whom any correspondence should be addressed.

E-mail: dsivak@sfu.ca

Keywords: molecular motors, collective transport, Langevin equation, stochastic thermodynamics, fluctuations

Abstract

Motor-driven intracellular transport of organelles, vesicles, and other molecular cargo is a highly collective process. An individual cargo is often pulled by a team of transport motors, with numbers ranging from only a few to several hundred. We explore the behavior of these systems using a stochastic model for transport of molecular cargo by an arbitrary number N of motors obeying linear Langevin dynamics, finding analytic solutions for the N-dependence of the velocity, precision of forward progress, energy flows between different system components, and efficiency. In two opposing regimes, we show that these properties obey simple scaling laws with N. Finally, we explore trade-offs between performance metrics as N is varied, providing insight into how different numbers of motors might be well-matched to distinct contexts where different performance metrics are prioritized.

1. Introduction

Living organisms are fundamentally out-of-equilibrium physical systems [1] characterized by sustained spatial inhomogeneities. To maintain this nonequilibrium state, organisms must constantly consume energy and transport material at several different lengthscales, including within individual cells. Intracellular transport is achieved using a plethora of different methods including passive and active diffusion, advection, ion pumps, and motor-driven transport [2]. These transport processes are characterized by unavoidable stochasticity as well as the overdamped motion inherent to the low-Reynolds-number regime these systems inhabit [3].

Motor proteins (also referred to as 'transport motors' or just 'motors') are integral components of eukaryotic cells, with a wide range of functions including transport of large macromolecular cargo over significant distances [4]. These motors transduce chemical energy, generally in the form of ATP, into net mechanical motion in a preferred direction [5]. Indeed, motor proteins can be thought of and modeled as nanoscale thermodynamic engines, whose behavior is characterized by stochastic mechanical and chemical dynamics [6]. Individual transport motors can reach speeds as high as $\sim 8\ \mu\text{m s}^{-1}$ [7] and make forward progress while pulling against forces on the order of ~ 6 pN [8]. Particularly well-characterized examples include kinesin and dynein motors pulling vesicles along microtubules [9], and myosin motors pulling on actin filaments to contract muscle tissue [10].

Motor proteins within cells often work collectively to transport large organelles such as mitochondria [4, 11], or even chromosomes during mitosis and meiosis [12]. Experimental determination of the number N of motors attached to a given cargo is generally challenging; nonetheless, recent studies have successfully measured N by identifying discrete peaks in a distinctly multimodal velocity distribution [13, 14] for small numbers of motors, or using more complex techniques such as quantitative immunoblots and immunoelectron microscopy [11]. Experimental investigations both *in vivo* and *in vitro* have found widely varying numbers N of motors coupled to a single cargo. In some cases, only a single motor [15] or a few motors [13] per cargo is observed, but experiments have observed as many as 200 motors bound to large organelles [11]. Likewise, in actomyosin filaments in muscle tissue, on the order of 100 motors are attached

to each actin filament [16]. Collective-transport systems can also be engineered *in vitro* [17]; in this setting the number of motors can be controlled more precisely, for example using DNA scaffolds [18, 19].

Simple phenomenological models for transport-motor dynamics (such as the classical linear force–velocity relationship [15, 20]) has been extended to multiple motors, for example by assuming equal load-sharing [13, 14]. These models provide a good first approximation to the dynamics of multi-motor systems, and can be extended to include, for example, motor binding and unbinding kinetics [21, 22]. These types of models assume that the motors pull against a constant force, rather than the stochastic frictional drag that would occur for a loosely coupled diffusive cargo. However, analysis of transport by single motors has shown that pulling a diffusing cargo and pulling against a constant force lead to qualitatively different transport behavior [23, 24]. Researchers have proposed and explored several dynamical models for transport of diffusive cargo by multiple motors [25–30]. These approaches rely primarily on numerical simulation, and as such are limited by computational resources to exploring systems with relatively small numbers of motors.

In studying intracellular transport, an important goal is to understand how systems can be tuned to improve performance. Relevant performance metrics vary based on the context, but may include cargo velocity, rate of chemical energy consumption, transport efficiency, and precision [5]. The dependence of these and other performance metrics on the number of motors is of clear interest, and has not yet been systematically investigated.

In this article we introduce a simple, thermodynamically consistent, stochastic model for the collective transport of diffusive molecular cargo by an arbitrary number N of motors. This model has a key advantage over other recent theoretical and computational approaches: we can solve it analytically for arbitrary N, allowing us to explore system behavior over many orders of magnitude of motor numbers. We derive N-dependent expressions for several performance metrics, and explicitly calculate all thermodynamic energy flows between different system components and thermal and chemical reservoirs. This allows us to derive simple analytic expressions for efficiency both of the whole system and of individual motors. In two opposing regimes we identify simple scaling laws that characterize the N-dependence of these properties. Finally, we derive fundamental trade-offs among these performance metrics, thereby pointing to design principles for collective motor-driven transport.

2. Model and theory

We consider a diffusive cargo coupled to N identical transport motors, with motion resolved in one dimension. Each motor interacts only with the cargo via a molecular linker, and is characterized by a mechanochemical cycle through which it transduces chemical power into directed forward motion. The cargo undergoes Brownian motion subject to coupling forces from each motor via the respective linker. Figure 1 illustrates the system.

We focus on the limiting regime in which the time evolution of the system is independent of the initial conditions, which we call its steady state. Mathematically, the relevant limit is that the time greatly exceeds the system's longest relaxation time ($t \gg \tau_{\text{relax}}$). In our general discussion, we assume that this limit exists, and that in the steady state, system properties such as the velocity, efficiency, energy flows and entropy production all have well-defined constant average values. The specific model we introduce below satisfies these assumptions.

2.1. Model

We model the cargo and motors as overdamped Brownian particles diffusing (with respective diffusivities D_{c} and D_{m}) in a potential landscape. x_{c} and x_i describe the positions of the cargo and ith motor. For mathematical simplicity we treat the cargo as a single point, but our model describes equally well (through a linear change of variables) motors attached at different points to a rigid cargo. The system is isothermal and in contact with a thermal reservoir at inverse temperature $\beta \equiv (k_{\text{B}}T)^{-1}$. We assume that both cargo and motor dynamics satisfy the fluctuation–dissipation relation: the friction coefficients for the cargo (ζ_{c}) and motors (ζ_{m}) are related to their respective diffusivities by $\beta\zeta_{\text{c}}D_{\text{c}} = 1 = \beta\zeta_{\text{m}}D_{\text{m}}$.

Each motor is subject to chemical driving due to nonequilibrium environmental concentrations of molecules, often ATP, ADP, and phosphate, and further experiences an underlying periodic energy landscape due to interactions with the substrate it walks along. To simplify the analysis, we assume that the scale of this energy landscape (the heights of the barriers separating meta-stable states) are small compared to the magnitude of the chemical driving. This leads to the motors experiencing a flat, downward-sloping energy landscape, which can be thought of as a constant force f_{chem} propelling each motor in a preferred direction. We further assume tight coupling between chemical-energy consumption and forward motor motion.

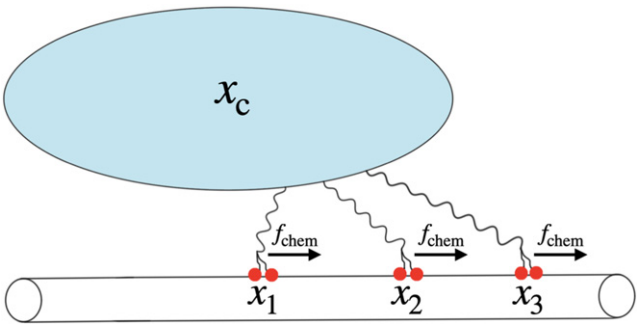

Figure 1. Collective-transport system comprising a single diffusive cargo coupled to N (here $N = 3$) motor proteins moving along a linear substrate. x_c indicates the cargo position, and x_i the position of the ith motor. Each motor experiences chemical driving force f_{chem}.

We model each linker coupling one motor to the cargo as a Hookean spring with zero rest length, dominated by the along-filament displacement, thus with interaction potential $U_i(x_c, x_i) = \frac{1}{2}\kappa(x_i - x_c)^2$. This is a common assumption in modeling approaches [24, 28] and experimentally well-supported for kinesin linkers [31].

This model system dynamically evolves according to $N + 1$ coupled Langevin equations,

$$\dot{x}_c = \beta D_c \kappa \sum_{i=1}^{N} (x_i - x_c) + \eta_c, \tag{1a}$$

$$\dot{x}_i = \beta D_m \left[f_{chem} - \kappa(x_i - x_c) \right] + \eta_i, \quad i = 1, \ldots, N. \tag{1b}$$

Here $\eta_c(t)$ and $\eta_i(t)$ are independent Gaussian noises with means and variances

$$\langle \eta_c(t) \rangle = 0, \tag{2a}$$

$$\langle \eta_i(t) \rangle = 0 \tag{2b}$$

$$\langle \eta_c(t)\eta_c(t') \rangle = 2D_c\delta(t - t'), \tag{2c}$$

$$\langle \eta_i(t)\eta_j(t') \rangle = 2D_m\delta_{ij}\delta(t - t'), \tag{2d}$$

$$\langle \eta_c(t)\eta_i(t') \rangle = 0. \tag{2e}$$

Here δ_{ij} is the Kronecker delta function and $\delta(t - t')$ the Dirac delta function.

The single-motor dynamics (1b) produce average motion equivalent to the linear force–velocity relation typically observed experimentally for kinesin motors under constant forces less than their stall force [15, 20] (where most of our analysis takes place),

$$\langle v \rangle = v_{max} \left(1 - \frac{f}{f_s} \right), \tag{3}$$

for stall force $f_s = f_{chem}$, maximum velocity $v_{max} = \beta D_m f_{chem}$, and force $f = \kappa\langle x_i - x_c \rangle$ acting on the motor.

2.2. Thermodynamics

Our model is thermodynamically consistent, so we use the tools of stochastic thermodynamics [6] to analyze the energy flows between various system components. Each subsystem (cargo or motor) exchanges heat with a thermal reservoir at inverse temperature β, and each motor exchanges chemical energy with reservoirs characterized by constant chemical potentials. The ith motor exchanges energy with the cargo through their interaction potential U_i.

The ith motor consumes average chemical power

$$P_{\to M_i} = \langle \dot{x}_i \circ f_{chem} \rangle \tag{4}$$

and transmits average power

$$P_{M_i \to C} = \left\langle \dot{x}_i \circ \frac{\partial U_i}{\partial x_i} \right\rangle \tag{5}$$

to the cargo through the linker. Equation (4) implicitly assumes each tightly couples its chemical and mechanical degrees of freedom, consistent with experimental findings for kinesin motors [32, 33]. The respective average rates of heat flow from the thermal reservoir into the cargo and ith motor are

$$\dot{Q}_{\to \mathrm{C}} = \left\langle \dot{x}_\mathrm{c} \circ \sum_{i=1}^{N} \frac{\partial U_i}{\partial x_\mathrm{c}} \right\rangle, \tag{6a}$$

$$\dot{Q}_{\to \mathrm{M}_i} = \left\langle \dot{x}_i \circ \left[\frac{\partial U_i}{\partial x_i} - f_\mathrm{chem} \right] \right\rangle. \tag{6b}$$

Here, angled brackets denote ensemble averages over stochastic fluctuations, and the product (indicated by the symbol '$\circ$') between $\dot{x}_\mathrm{c}$ or $\dot{x}_i$ and other quantities is interpreted using the Stratonovich rule so that the ensemble averages can be evaluated using the methods outlined in [6]. Transport systems are highly processive, so we focus on average energy flows, ignoring higher moments that are less salient at long durations.

At steady state, the average internal energy of each subsystem is constant, giving subsystem-specific first laws

$$0 = \sum_{i=1}^{N} P_{\mathrm{M}_i \to \mathrm{C}} + \dot{Q}_{\to \mathrm{C}}, \tag{7a}$$

$$0 = P_{\to \mathrm{M}_i} - P_{\mathrm{M}_i \to \mathrm{C}} + \dot{Q}_{\to \mathrm{M}_i}, \quad \forall\, i \in 1, \ldots, N. \tag{7b}$$

The second law bounds the total entropy production rate $\dot{\Sigma}$ (here equaling the total chemical power $P_\mathrm{chem} = \sum_i P_{\to \mathrm{M}_i}$) and hence the heat flows [34]:

$$0 \leqslant \dot{\Sigma} = P_\mathrm{chem} \tag{8a}$$

$$= -\dot{Q}_{\to \mathrm{C}} - \sum_{i=1}^{N} \dot{Q}_{\to \mathrm{M}_i}. \tag{8b}$$

3. Results

3.1. Solution

Equation (1) constitute a linear system of coupled Langevin equations, and as such are in general analytically solvable, with solution a multivariate Gaussian. Thus it suffices to solve for the mean vector and covariance matrix of the whole system, the components of which satisfy a set of coupled linear ordinary differential equations [35, section 3.2]. Since the N motors dynamically evolve according to identical stochastic equation (1b), their marginal position distributions are identical. As a result, there are only two unique means ($\langle x_i \rangle$ and $\langle x_\mathrm{c} \rangle$) and four unique covariances ($\mathrm{Cov}(x_\mathrm{c}, x_\mathrm{c})$, $\mathrm{Cov}(x_\mathrm{c}, x_i)$, $\mathrm{Cov}(x_i, x_i)$, and $\mathrm{Cov}(x_i, x_j)$), all of which vary with time. This symmetry permits exact solution without specifying N. Appendix A details the unwieldy analytic expressions.

The distributions of $\{x_i(t)\}_{i=1}^N$ and $x_\mathrm{c}(t)$ are time-dependent, so we change to a set of N variables, $\Delta x_i(t) = x_i(t) - x_\mathrm{c}(t)$, that at steady state converge to a time-independent joint distribution, a multivariate Gaussian with means and covariances

$$\langle \Delta x_i \rangle = \frac{f_\mathrm{chem}}{\kappa} \left(1 + N \frac{D_\mathrm{c}}{D_\mathrm{m}} \right)^{-1}, \tag{9a}$$

$$\mathrm{Cov}(\Delta x_i, \Delta x_j) = \frac{1}{\beta \kappa} \delta_{ij}. \tag{9b}$$

This time-independent distribution is sufficient to compute many steady-state properties of interest.

For our model we find that the off-diagonal entries of the stationary covariance matrix, $\mathrm{Cov}(\Delta x_i, \Delta x_j)$ for $i \neq j$, are zero: fluctuations in the relative position of one motor are uncorrelated with the relative positions of the other motors. We do not expect this particular result to generalize; for example, collective-transport models with discrete motor motion [28] have found non-zero off-diagonal covariances at small N. Regardless, the results presented below depend only on diagonal terms and are independent of off-diagonal covariances.

The system relaxation time is $\tau_\mathrm{relax} = [\beta \kappa (D_\mathrm{m} + N D_\mathrm{c})]^{-1}$. Appendix B provides parameter estimates indicating that this is at most $\sim$0.02 s for kinesin pulling molecular cargo, and generally at least an order of

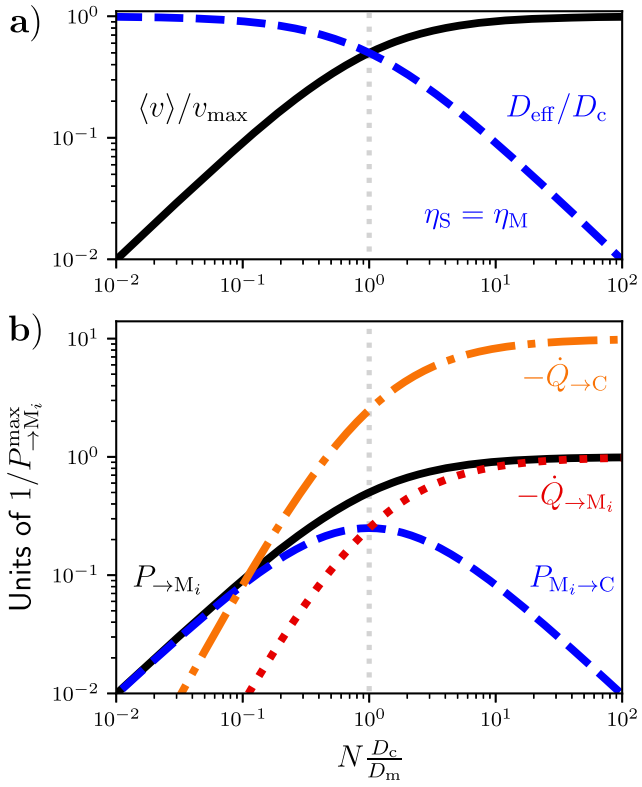

Figure 2. (a) Scaled velocity $\langle v \rangle / v_{\max}$ (equation (10)) and effective diffusivity $D_{\mathrm{eff}}/D_{\mathrm{c}}$ (equation (11)) (equal to the efficiency $\eta \equiv \eta_{\mathrm{M}} = \eta_{\mathrm{S}}$ (equation (18))) as functions of the number N of motors scaled by the diffusivity ratio $D_{\mathrm{m}}/D_{\mathrm{c}}$. (b) Ensemble-averaged energy flows $P_{\to \mathrm{M}_i}$ (equation (14)), $P_{\mathrm{M}_i \to \mathrm{C}}$ (equation (15)), $\dot{Q}_{\to \mathrm{M}_i}$ (equation (16)), and $\dot{Q}_{\to \mathrm{C}}$ (equation (17)) as functions of N scaled by $D_{\mathrm{c}}/D_{\mathrm{m}}$. All energy flows are scaled by the chemical power consumption $P^{\max}_{\to \mathrm{M}_i} = f_{\mathrm{chem}} v_{\max}$ of a single motor at maximum velocity. For $\dot{Q}_{\to \mathrm{C}}$ we use $D_{\mathrm{c}}/D_{\mathrm{m}} = 1/10$; all other energy flows depend solely on the quantity $ND_{\mathrm{c}}/D_{\mathrm{m}}$.

magnitude smaller. This corresponds to a distance of at most 40 nm for kinesin motors at maximum velocity. Given the short distance over which relaxation to steady state occurs, and the high processivity of motor-driven transport systems (kinesin can travel up to several micrometers before detaching [36]), we exclusively focus on the steady state.

The dimensionless parameter combination $ND_{\mathrm{c}}/D_{\mathrm{m}}$ appears in equation (9a) and in many of the results shown later on, constituting a key quantity for understanding the system behavior. For intracellular transport of vesicles or organelles the diffusivity ratio $D_{\mathrm{c}}/D_{\mathrm{m}}$ is typically $\sim 10^{-3}$–10^{0}, depending on the size of the cargo (see appendix B). Since N can range from one to several hundred, we focus our explorations on the range $ND_{\mathrm{c}}/D_{\mathrm{m}} \in [10^{-3}, 10^{3}]$.

3.2. Scaling behavior

3.2.1. Dynamical properties

At steady state, the cargo and each motor have equal velocity, $\langle v_{\mathrm{c}} \rangle \equiv \lim_{t\to\infty} \langle x_{\mathrm{c}}(t) - x_{\mathrm{c}}(0) \rangle / t = \lim_{t\to\infty} \langle x_i(t) - x_i(0) \rangle / t \equiv \langle \mathrm{v}_{\mathrm{m}} \rangle \equiv \langle \mathrm{v} \rangle$. Evaluating this limit yields a simple expression for the N-dependent mean system velocity:

$$\langle \mathrm{v} \rangle = \mathrm{v}_{\max} \left(1 + \frac{D_{\mathrm{m}}}{N D_{\mathrm{c}}} \right)^{-1}. \tag{10}$$

For $N \ll D_{\mathrm{m}}/D_{\mathrm{c}}$, the mean velocity grows linearly with N, so adding more motors proportionally increases the system velocity. As N grows much larger than $D_{\mathrm{m}}/D_{\mathrm{c}}$, however, the steady-state velocity asymptotically approaches maximum velocity $\mathrm{v}_{\max} = \beta D_{\mathrm{m}} f_{\mathrm{chem}}$ (the mean velocity of an uncoupled motor) as $\langle \mathrm{v} \rangle \approx \mathrm{v}_{\max} \left[1 - D_{\mathrm{m}}/(ND_{\mathrm{c}}) \right]$. Thus no matter how many motors are coupled to the cargo, the mean velocity of the aggregate motor–cargo system never exceeds that of an unladen motor. This mean velocity (as well as the maximum velocity) scales linearly with the chemical driving force f_{chem}. Figure 2(a) shows normalized velocity $\langle \mathrm{v} \rangle / \mathrm{v}_{\max}$ as a function of N.

While $\langle \mathrm{v} \rangle$ gives the average motion, our model (like all transport at the cellular level) is inherently stochastic. As such, the average velocity is not sufficient to fully describe system behavior, even at steady

state. The effective cargo diffusivity D_{eff} quantifies the rate at which the variance of forward progress grows at steady state:

$$D_{\text{eff}} \equiv \lim_{t\to\infty} \frac{\langle x_{\text{c}}^2\rangle - \langle x_{\text{c}}\rangle^2}{2t} \tag{11a}$$

$$= \left(\frac{1}{D_{\text{c}}} + \frac{N}{D_{\text{m}}}\right)^{-1}. \tag{11b}$$

This expression can be understood by noting that the effective friction coefficient for the system, $\zeta_{\text{eff}} = 1/\beta D_{\text{eff}}$, is simply the sum of the friction coefficients for the motors and cargo. This interpretation is consistent with a recent theoretical study of collective transport of a diffusive cargo using discrete motor dynamics, which similarly found that the contribution from the motors to the effective friction coefficient of the system scales linearly with the number N of motors for the small range explored [37]. Previous work using a simpler phenomenological model also suggested that the effective friction coefficient of a collection of motors should be proportional to N [38].

Figure 2(a) shows D_{eff} as a function of N. While the velocity increases with the number of motors, the effective diffusivity decreases, indicating that a larger number of motors tightens the distribution of cargo-transport distances. Writing the mean velocity as $\langle v\rangle = \beta D_{\text{eff}}\left(N f_{\text{chem}}\right)$ reveals that the effective dynamics of the system are simply those of a single diffusive particle (with diffusivity D_{eff}) under a constant driving force $N f_{\text{chem}}$.

The system stochasticity can alternatively be quantified by the coefficient of variation θ [39] or the Fano factor ϕ [24]. The coefficient of variation (CV) of cargo position is

$$\theta \equiv \frac{\sqrt{\langle x_{\text{c}}^2\rangle - \langle x_{\text{c}}\rangle^2}}{\langle x_{\text{c}}\rangle} \tag{12a}$$

$$= \sqrt{2\left(\frac{1}{D_{\text{c}}} + \frac{N}{D_{\text{m}}}\right)}\,\frac{D_{\text{c}}}{N D_{\text{m}}}\,\frac{1}{\beta f_{\text{chem}}}\,t^{-1/2}. \tag{12b}$$

For small $N \ll D_{\text{m}}/D_{\text{c}}$ the coefficient of variation scales as N^{-1}, while for large $N \gg D_{\text{m}}/D_{\text{c}}$, $\theta \propto N^{-1/2}$. Thus this measure of the variation in forward progress can be made arbitrarily small with sufficiently large $N D_{\text{c}}/D_{\text{m}}$, but with diminishing returns for larger N.

The steady-state Fano factor is

$$\phi \equiv \frac{\langle x_{\text{c}}^2\rangle - \langle x_{\text{c}}\rangle^2}{\langle x_{\text{c}}\rangle} = \frac{2}{N\beta f_{\text{chem}}}. \tag{13}$$

Similarly to D_{eff}, ϕ decreases (and hence the precision increases) with the number of motors, scaling as $\phi \propto N^{-1}$. Here adding motors decreases the variance of forward progress while increasing the velocity, leading to a Fano factor that decreases with N. For $N = 1$ motor, equation (13) recovers the Fano factor previously calculated in the limit of low cargo diffusivity [24] for a single motor.

The addition of motors can be thought of as having an 'averaging' effect on the dynamics. The precision (as quantified by θ or ϕ) also increases with the chemical driving force f_{chem} on each motor. Figure C1 in appendix C shows the three stochasticity metrics.

3.2.2. Thermodynamic properties

We also exactly calculate steady-state ensemble averages of all energy flows into and out of each subsystem. The mean chemical power (4) to each motor is

$$\beta P_{\to \text{M}_i} = N D_{\text{c}}\left(1 + N\frac{D_{\text{c}}}{D_{\text{m}}}\right)^{-1}\left(\beta f_{\text{chem}}\right)^2 \tag{14a}$$

$$= \beta f_{\text{chem}}\langle v\rangle. \tag{14b}$$

We multiply the energy flows by the inverse temperature β so that quantities have units of s^{-1}. In keeping with our assumption of tight mechanochemical coupling, the power consumption is simply the chemical driving force multiplied by the motor velocity. Since the motors are identical, the total chemical power consumption is simply $P_{\text{chem}} = N P_{\to \text{M}_i}$. Likewise, the average rate of work performed on the cargo by each motor is

$$\beta P_{\text{M}_i \to \text{C}} = N D_{\text{c}}\left(1 + N\frac{D_{\text{c}}}{D_{\text{m}}}\right)^{-2}\left(\beta f_{\text{chem}}\right)^2 \tag{15a}$$

$$= \frac{\langle v\rangle^2}{N D_{\text{c}}}. \tag{15b}$$

The total power $\sum_i P_{\mathrm{M}_i\to\mathrm{C}} = \langle v\rangle^2/D_\mathrm{c}$ transferred from the motors to the cargo increases monotonically with N and reaches a finite maximum value. $P_{\mathrm{M}_i\to\mathrm{C}}$ for a single motor is non-monotonic in N, as shown in figure 2(b). In particular, $P_{\mathrm{M}_i\to\mathrm{C}} \propto N$ for $N \ll D_\mathrm{m}/D_\mathrm{c}$ and $\propto N^{-1}$ for $N \gg D_\mathrm{m}/D_\mathrm{c}$. This is because for large N, when the cargo reaches maximum velocity and thus a constant rate of heat dissipation, the sum $\sum_i P_{\mathrm{M}_i\to\mathrm{C}} = -\dot{Q}_{\to\mathrm{C}}$ must reach a constant value as well. Dividing this nearly constant total power among an increasing number of motors means that $P_{\mathrm{M}_i\to\mathrm{C}}$ decreases. Thus the power flow from each individual motor to the cargo is maximized at an intermediate $N^* = D_\mathrm{m}/D_\mathrm{c}$.

The average heat flow into each motor is

$$\beta\dot{Q}_{\to\mathrm{M}_i} = -N^2\frac{D_\mathrm{c}^2}{D_\mathrm{m}}\left(1+N\frac{D_\mathrm{c}}{D_\mathrm{m}}\right)^{-2}\left(\beta f_\mathrm{chem}\right)^2 \tag{16a}$$

$$= -\frac{\langle v\rangle^2}{D_\mathrm{m}}, \tag{16b}$$

and the heat flow into the cargo is

$$\beta\dot{Q}_{\to\mathrm{C}} = -N^2 D_\mathrm{c}\left(1+N\frac{D_\mathrm{c}}{D_\mathrm{m}}\right)^{-2}\left(\beta f_\mathrm{chem}\right)^2 \tag{17a}$$

$$= -\frac{\langle v\rangle^2}{D_\mathrm{c}}. \tag{17b}$$

The subsystem-specific heat flows are, on average, given by the friction coefficient (e.g. $\zeta_\mathrm{c} = 1/\beta D_\mathrm{c}$ for the cargo) multiplied by the mean velocity squared, the result we would expect for the frictional energy dissipation of an overdamped particle moving at constant velocity $\langle v\rangle$. The sum of the heat flows over all $N+1$ subsystems represents the total energy dissipation of the system at steady state. As indicated by equation (8), all of the chemical energy consumed by the motors is either dissipated directly by the motors as heat (due to loose coupling to the cargo) or transduced into mechanical work on the cargo which is then dissipated by the cargo as heat.

Figure 2(b) shows how these four steady-state energy flows depend on the number N of motors, manifesting two regimes. For $N \ll D_\mathrm{m}/D_\mathrm{c}$, the heats $-\dot{Q}_{\to\mathrm{M}_i}$ and $-\dot{Q}_{\to\mathrm{C}}$ scale as N^2, while the chemical power $P_{\to\mathrm{M}_i}$ to each motor and the power $P_{\mathrm{M}_i\to\mathrm{C}}$ from each motor to the cargo scale linearly with N. For $N \gg D_\mathrm{m}/D_\mathrm{c}$, the chemical power to each motor as well as the two heats asymptotically approach constants. For sufficiently large N, each motor's heat roughly equals its chemical power consumption, as the power per motor transferred through the coupling decays as N^{-1}.

All energy flows display the same quadratic dependence on the chemical driving force. This is reminiscent of linear irreversible thermodynamics, where rates of entropy production (and thus heat dissipation) are quadratic in the thermodynamic driving forces [40]. This is true for our system on average due to the linearity of equations (1a) and (1b), even with the inherent stochasticity.

The steady-state energy flows (14)–(17) are all independent of the coupling strength κ, despite the steady-state distributions for the separation distances Δx_i depending strongly on κ. To understand this surprising result, consider the average force an individual motor pulls against, $\kappa\langle\Delta x_i\rangle$, for separation distance $\Delta x_i \equiv x_i - x_\mathrm{c}$. Equation (9a) shows that $\langle\Delta x_i\rangle \propto 1/\kappa$, so the mean force on the motor is independent of the coupling strength. Since the motor velocity is also independent of the coupling strength, the mean power output of each motor (roughly the mean velocity multiplied by the mean opposing force) is independent as well. The power consumption $P_{\to\mathrm{M}_i}$ is likewise independent of κ for the same reason. From the first law (7) the system only has three independent energy flows, so the other energy flows must thus also be independent of κ.

We consider several different metrics of steady-state energetic efficiency. Thermodynamic efficiency is the ratio of output power to input power. Since the system does not perform any thermodynamic work as output, and the input power P_chem is always positive, the full system's thermodynamic efficiency is zero; however, the thermodynamic efficiency $\eta_\mathrm{M} \equiv P_{\mathrm{M}_i\to\mathrm{C}}/P_{\to\mathrm{M}_i}$ of each motor subsystem is positive.

The Stokes efficiency $\eta_\mathrm{S} \equiv \zeta_\mathrm{c}\langle v\rangle^2/P_\mathrm{chem}$ evaluates systems whose only functional output is directed motion against viscous friction [41]. We consider only the frictional drag on the cargo (with drag coefficient ζ_c), assuming that directed cargo motion is ultimately the main purpose of the system. This system has equal Stokes efficiency and motor efficiency:

$$\eta_\mathrm{M} = \eta_\mathrm{S} = \left(1+N\frac{D_\mathrm{c}}{D_\mathrm{m}}\right)^{-1}. \tag{18}$$

Table 1. Performance metrics' asymptotic scaling with N.

Metric	$N \ll D_m/D_c$	$N \gg D_m/D_c$
$\langle \mathrm{v} \rangle$	$\propto N$	$\approx v_{\max}\left[1 - D_m/(ND_c)\right]$
θ	$\propto N^{-1}$	$\propto N^{-1/2}$
P_{chem}	$\propto N^2$	$\propto N$
$\eta_{S/M}$	$\approx 1 - ND_c/D_m$	$\propto N^{-1}$

Figure 2(a) shows efficiency as a function of N: for small ND_c/D_m, the efficiency is $\approx 1 - ND_c/D_m$, while for $ND_c/D_m \gg 1$ the efficiency scales as N^{-1}. For a given diffusivity ratio D_c/D_m, the efficiency for any N is upper bounded by $\eta_{\max} = \left(1 + D_c/D_m\right)^{-1}$ since N is lower bounded by unity. Thus, for example, a system with $D_c = D_m$ can achieve at most 50% efficiency. This efficiency can be re-written in terms of the system's effective diffusivity as

$$\eta_M = \eta_S = \frac{D_{\mathrm{eff}}}{D_c}, \tag{19}$$

which exactly saturates an upper bound proven for the Stokes efficiency of transport by a single motor [42].

Table 1 summarizes the scaling with N of our key performance metrics in the two limiting regimes.

3.3. Performance trade-offs

The previous section outlined the separate N-dependence of different performance metrics; however, these quantities are not independent, instead posing trade-offs parameterized by N. We examine the trade-offs between all pairs of dynamical and thermodynamic properties from table 1, and find that several pairs of desirable properties cannot be simultaneously attained.

The mean transport velocity and the total chemical power consumption of the motors are related by

$$\frac{P_{\mathrm{chem}}}{P^{\max}_{\to M_i}} = \frac{D_m}{D_c} \frac{\left(\langle \mathrm{v} \rangle / \mathrm{v}_{\max}\right)^2}{1 - \langle v \rangle / \mathrm{v}_{\max}}. \tag{20}$$

Figure 3(a) illustrates this trade-off as N is varied, for several different diffusivity ratios. For $N \ll D_m/D_c$, the total chemical input power scales as the square of the average velocity $\langle v \rangle$. At $N = D_m/D_c$ the velocity is half its maximum; beyond this velocity the required chemical power skyrockets, scaling as $P_{\mathrm{chem}} \propto \left(v_{\max} - \langle v \rangle\right)^{-1}$ for $N \gg D_m/D_c$.

The total power consumption and coefficient of variation (12) are inversely related,

$$P_{\mathrm{chem}} = (2/t)\theta^{-2}, \tag{21}$$

for all N and D_c/D_m. Figure 3(b) illustrates this trade-off, which features scaling behavior consistent across the regimes of large and small N. Arbitrarily high precision (low θ) can be achieved in this collective-transport system, but at the cost of power consumption that increases without bound.

Comparing (10) and (18), the efficiency and scaled velocity obey a simple relation:

$$\eta_{S/M} + \frac{\langle v \rangle}{v_{\max}} = 1, \tag{22}$$

where $\eta_{S/M}$ can be either the Stokes or motor efficiency, since they are equal for this system. Figure 3(c) shows this trade-off. Our collective-transport system cannot simultaneously achieve high efficiency and near-maximum velocity. Further, depending on the diffusivity ratio only certain efficiencies are achievable: those with $\eta_{S/M} \leqslant \eta_{\max} = \left(1 + D_c/D_m\right)^{-1}$. Notably, 50% efficiency and half-maximal velocity can always be achieved at $N = D_m/D_c$.

Finally we consider the trade-off between efficiency and precision (quantified by coefficient of variation θ),

$$\theta\, \mathrm{v}_{\max} \sqrt{\frac{t}{2D_c}} = \frac{\sqrt{\eta_{S/M}}}{1 - \eta_{S/M}}. \tag{23}$$

Figure 3(d) shows that high efficiency and high precision (low CV) are not simultaneously achievable. This suggests that to maximize efficiency systems must exploit thermal fluctuations, leading to a decrease in precision. Note that the transition from near-zero to near-unit efficiency occurs over a small range of CVs around $N = D_m/D_c$.

Insets in figures 3(a), (b) and (d) show that scaling the power consumption and coefficient of variation by factors of the diffusivity ratio D_c/D_m collapses the separate curves for distinct D_c/D_m onto single master

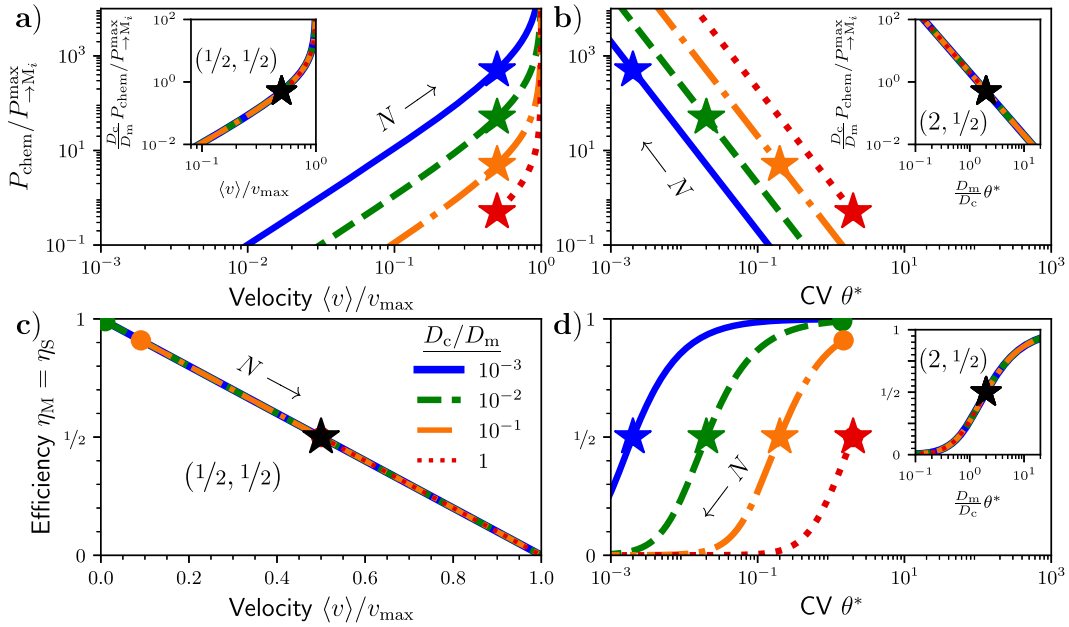

Figure 3. Trade-offs between (a) scaled chemical power consumption $P_{\text{chem}}/P^{\max}_{\to M_i}$ and scaled mean velocity $\langle v\rangle/v_{\max}$, (b) $P_{\text{chem}}/P^{\max}_{\to M_i}$ and scaled coefficient of variation $\theta^* = \theta v_{\max}\sqrt{t/D_c}$, (c) efficiency $\eta_S = \eta_M$ and $\langle v\rangle/v_{\max}$, and (d) $\eta_S = \eta_M$ and θ^*, as the number N of motors is varied, for different diffusivity ratios D_c/D_m. Stars: $N = D_m/D_c$. Circles: maximum efficiencies for respective diffusivity ratios, $\eta_{\max} = (1 + D_c/D_m)^{-1}$, realized for $N = 1$. Insets in (a), (b) and (d) show that scaling the power consumption and coefficient of variation by factors of D_c/D_m collapses the curves for different diffusivity ratios onto single master curves. Numbers in parentheses indicate coordinates of black stars (where $ND_c/D_m = 1$). All curves terminate at points where $N = 1$, so that we always show real numbers of motors.

curves. Thus the qualitative nature of the trade-offs described here are independent of the relative diffusivities of the motors and cargo.

These performance trade-offs suggest that collective-transport systems where different performance metrics are prioritized should have different numbers of motors if N can be adjusted to tune performance. For systems in which maximum velocity and high precision are preferred, optimization would drive systems towards the $N \gg D_m/D_c$ regime. This would however come with the cost of high power consumption and decreased efficiency. If instead highly efficient directed transport on a small power budget is favored, then optimal systems would have $N \ll D_m/D_c$ at the cost of slow and imprecise transport.

3.4. Generalization

Many of our results extend to more general models of motor dynamics. As an example, we relax the assumption that the chemical driving force is much larger than the scale of the motor's energy landscape, and add a periodic sinusoidal potential-energy landscape to each motor (see appendix D for details). This continuous model, inspired by similar models of other molecular machines [23, 43], produces motor dynamics qualitatively similar to commonly used discrete-step models [26, 28].

Figure D1 shows for this more complex model the scaling with N of the mean velocity $\langle v\rangle$, chemical power consumption P_{chem}, and Stokes efficiency η_S, for a variety of barrier heights. (Calculating the coefficient of variation for large N is computationally intractable.) The scaling laws in the limiting regimes of large and small N (outlined in table 1) still accurately reflect the limiting scaling behavior for this generalization. As a direct result of the scaling laws generalizing, the performance trade-offs [figures 3(a) and (c)] also apply more generally, at least qualitatively: even under more general motor dynamics, desirable pairs of properties such as high velocity and high efficiency or high velocity and low power consumption remain mutually exclusive.

4. Discussion

In this article we introduced a simple model for collective intracellular transport by an arbitrary number of transport motors. This model is stochastic, thermodynamically consistent, and can be solved analytically for arbitrary motor number N. Using this model we derived analytic expressions for several steady-state properties, including dynamic properties such as mean velocity, effective diffusivity, and precision, as well as thermodynamic quantities such as power, heat, and efficiency. We found qualitatively different

N-dependence for these quantities in the two opposing regimes of high and low N (compared to the motor–cargo diffusivity ratio D_m/D_c), summarized by simple scaling laws (table 1). Our model should best reflect the physics of motors whose energy-landscape features are smaller in scale than the magnitude of their chemical driving, however our numerical explorations in appendix D suggest that many of our results generalize well beyond this regime.

We also examined trade-offs between several performance metrics that are expected to be generally important for real transport systems: many pairs of desirable properties, for example high velocity and high efficiency, are mutually exclusive in these systems. The trade-off between efficiency and velocity (figure 3(c)) has also been explored theoretically in other types of molecular machines [44, 45]. The incompatibility of high velocity and high efficiency seems to be a general feature of these types of systems, and has also been seen experimentally for myosin motors [7]. These findings are reminiscent of the thermodynamic uncertainty relation [46], which lower bounds the product of uncertainty and entropy production. At steady state our system saturates this bound, which may be a universal feature of linear systems with only one driving force [47] or systems described by Gaussian probability distributions [48]. This suggests that the performance trade-offs (especially figure 3(b)) may in fact be Pareto frontiers [49] for more general collective-transport systems.

Few experiments have measured exact numbers of motors in collective transport systems; nonetheless, motor numbers have indeed been measured, for example by identifying discrete peaks in a distinctly multimodal velocity distribution. Using this technique to study transport of beads by kinesin motors [13, 14], found a mean velocity roughly proportional to the number of motors, consistent with our predictions for the small-N regime; the bead diameter and solution viscosity indicate that these experiments had $N < D_c/D_m$. Similar experimental investigations have also found velocity to be a concave function of N, qualitatively consistent with our predictions [50]. Other experiments have varied the concentration of motor proteins in solution, a rough proxy for the number of motors per cargo. Kinesin motors attached to a substrate while transporting long microtubules [51, 52] produce velocity that is a concave function of motor concentration, as we predict; similar results have been found for myosin motors pulling actin filaments [16].

Using models similar to ours, but with discrete steps rather than continuous motor dynamics [25, 28], found a similar monotonic and concave functional dependence of the mean velocity $\langle \mathrm{v} \rangle$ on motor number N, although their findings are restricted to relatively small N. Likewise, [28] also found $D_{\mathrm{eff}} \propto 1/N$ for the greatest N they investigated. Another recent study [29] found that the total load capacity, or effective stall force, is N times the stall force for a single motor. We can easily incorporate into our model a constant external force f_{ext} pulling the cargo in the opposite direction of the chemical force driving the motors. To do this we simply add a term $-\beta D_c f_{\mathrm{ext}}$ to the left side of (1a), preserving analytic solubility of the dynamical equations. The mean velocity in this case is

$$\langle \mathrm{v} \rangle_{f_{\mathrm{ext}}} = \langle \mathrm{v} \rangle_0 \left(1 - \frac{f_{\mathrm{ext}}}{N f_{\mathrm{chem}}} \right), \tag{24}$$

where $\langle \mathrm{v} \rangle_0$ is the mean velocity for $f_{\mathrm{ext}} = 0$ given by equation (10). From this we identify the stall force $f_s = N f_{\mathrm{chem}}$ which scales linearly with the number of motors, independent of the diffusivity ratio.

Throughout this article we treated the number N of active motors per cargo as fixed, despite the fact that in real transport systems motor proteins are constantly binding and unbinding to both the cargo and the substrate. Our estimate $\tau_{\mathrm{relax}} < 0.02$ s of our system's relaxation time (section 3.1) is much shorter than estimates of 0.2–1 s for the motor binding and unbinding timescales of kinesin on microtubules [21]. Due to this timescale separation, we can treat the system as always in dynamical steady state at fixed N even when motors bind and unbind over longer timescales. Thus our steady-state results should still hold for temporally varying N. The convexity of these properties with respect to N determines the sign of the error resulting from computing steady-state quantities at a single average motor number $\langle N \rangle$ instead of considering a full distribution $P(N)$. For example, mean velocity is a concave function of N, so when N varies $\langle v\left(\langle N \rangle\right) \rangle$ overestimates the mean velocity $\langle \mathrm{v}(N) \rangle$. By contrast, the total power consumption is convex, so $\langle P_{\mathrm{chem}}(N) \rangle \geqslant P_{\mathrm{chem}}\left(\langle N \rangle\right)$. In appendix E we use a simple stochastic dynamical model of motor binding/unbinding to estimate that the error due to treating N as constant is small, especially when N is far from D_m/D_c.

Our model also ignores other possibly relevant effects such as motor–motor interactions and discretization of motor steps. Depending on the time- and lengthscales of resolution, motor proteins like kinesin can be thought of as taking discrete steps [53], in contrast to the continuous motion we assumed here. Nevertheless, treating the motor dynamics as continuous should be valid as long as the relaxation timescale for the motors is sufficiently separated from that of the cargo (either much larger or much smaller) so that the steady-state separation distance distribution (9) converges to the resulting equilibrium

distributions. This assumption is valid for both $N \gg D_m/D_c$ and $N \ll D_m/D_c$, but may break down for $N \approx D_m/D_c$, where system behavior may be more sensitive to the exact motor dynamics.

Interactions between motors may become relevant under certain conditions. Computational studies indicate the possibility of long-range cooperative interactions between kinesin motors through microtubules [54] as well as crowding effects such as traffic jams when large numbers of motors are present [55]. While we have not incorporated these effects into our model at present, generalizing our results using model-agnostic considerations from the theory of stochastic thermodynamics is a promising future direction.

Our model does break down under certain limiting conditions. Our analysis yields a mean velocity proportional to the chemical driving force acting on each motor. For kinesin motors hydrolyzing ATP, this is consistent with experimental findings at lower ATP concentrations, but not at high ATP concentrations where motor velocity saturates, with a cross-over at ATP concentrations on the order of 0.1 mM [32] (depending on the load the motor is pulling against). This discrepancy arises because we do not explicitly model the motor's mechanochemical cycle, implicitly treating the binding of ATP as the rate-limiting step. Reaction steps not dependent on the free-energy consumption should become rate-limiting at high ATP concentrations [56] leading to a saturating velocity. Our main results (the N-dependence and trade-offs of key performance metrics) are all independent of the magnitude of f_{chem}. Nonetheless, we expect our model to best capture the dynamics of real systems at lower ATP concentrations, in the linear-velocity regime. For systems with very large chemical driving forces, we expect the true maximum velocity of a single uncoupled motor to saturate, unlike our predicted $v_{\max} = \beta D_m f_{\text{chem}}$.

The performance trade-offs we derived in section 3.3 point to insights about optimization in collective-transport systems, as adjusting the number of motors per cargo can tune performance. This could be achieved, for example, by manipulating the motor concentration [57], adjusting the number of possible binding sites on the cargo [58], or using extra structural assemblies such as DNA scaffolds [18]. Depending on the regime the system inhabits, as determined by the dimensionless quantity ND_c/D_m, systems can either achieve fast and precise but energetically costly transport ($N \gg D_m/D_c$), or efficient but slow and imprecise transport ($N \ll D_m/D_c$). Ultimately, real systems have likely evolved to optimize complex combinations of the performance metrics we have considered here and others we have not, however estimating ND_c/D_m for *in vivo* systems may provide insight into which performance metrics are most important in specific systems.

Acknowledgments

The authors thank Emma Lathouwers and Jannik Ehrich (SFU Physics) for useful discussions, and Eric Jones and Nancy Forde (SFU Physics) for feedback on the manuscript. We thank the two anonymous reviewers whose comments and suggestions helped improve and clarify this article. This work was supported by a Natural Sciences and Engineering Research Council of Canada (NSERC) CGS Masters fellowship (MPL), a BC Graduate Scholarship (MPL), an NSERC Discovery Grant and Discovery Accelerator Supplement (DAS), and a Tier-II Canada Research Chair (DAS).

Data availability statement

The data that support the findings of this study are available upon reasonable request from the authors.

Appendix A. Analytic expressions for means and covariances

As detailed in section 3.1, the coupled Langevin equations (equations (1a) and (1b)) that describe the dynamics of our system are analytically solvable, and the solution for the probability distribution of the respective positions x_c and $\{x_i\}_{i=1}^N$ of the cargo and motors is a multivariate Gaussian. Starting from initial conditions $x_c = x_i = 0$ at $t = 0$, at steady state ($t \gg \tau_{\text{relax}}$) the mean cargo position and motor positions are

$$\langle x_c \rangle = \langle v \rangle t - \frac{N f_{\text{chem}}}{\kappa} \frac{D_{\text{eff}}^2}{D_m D_c}, \tag{A1a}$$

$$\langle x_i \rangle = \langle v \rangle t + \frac{f_{\text{chem}}}{\kappa} \left(\frac{D_{\text{eff}}}{D_c} \right)^2, \tag{A1b}$$

and the covariances are

$$\mathrm{Cov}(x_c, x_c) = 2D_{\mathrm{eff}}t + \frac{N}{\beta\kappa}\left(\frac{D_{\mathrm{eff}}}{D_m}\right)^2, \tag{A2a}$$

$$\mathrm{Cov}(x_c, x_i) = 2D_{\mathrm{eff}}t - \frac{1}{\beta\kappa}\frac{D_{\mathrm{eff}}^2}{D_m D_c}, \tag{A2b}$$

$$\mathrm{Cov}(x_i, x_j) = 2D_{\mathrm{eff}}t + \frac{1}{\beta\kappa}\left[\delta_{ij} - \frac{D_{\mathrm{eff}}^2}{D_m}\left(\frac{N}{D_m} + \frac{2}{D_c}\right)\right], \tag{A2c}$$

for Kronecker delta function δ_{ij}. Different initial conditions would produce different time-independent constant terms in (A1) and (A2); however for large times (in the steady-state limit) the constant terms are negligible compared to the terms linear in t. Regardless of initial conditions, the difference between the constant terms in (A1a) and (A1b) will always be the mean value of the separation distance, $\langle \Delta x_i \rangle$.

Appendix B. Parameter estimates

In this appendix we discuss relevant experimental measurements of the parameters in our model, namely the linker spring constant κ, the chemical driving force f_{chem}, and the respective motor and cargo diffusivities D_m and D_c.

Experimentally, kinesin linkers are well-approximated as Hookean springs with a zero rest length and a spring constant $\sim$0.5 pN nm^{-1} [31]. Similar behavior has been observed for the linkers of myosin V motors, which have an estimated spring constant of 0.2–0.4 pN nm^{-1} [59].

We estimate the chemical driving force f_{chem} in two ways. By noting the equivalence in equation (3) of f_{chem} with the single-motor stall force, we use experimental estimates of single-motor stall forces to estimate the chemical driving force. Kinesin motors have stall forces on the order of 5–8 pN [33], while myosin motors stall at forces as high as 15 pN [60]. (Note that the stall force monotonically increases with cellular ATP concentration.)

Likewise, due to tight coupling between chemical energy consumption and mechanical motion [32, 33], f_{chem} can also be thought of as a free-energy dissipation per unit distance. Kinesin, for example, hydrolyzes one molecule of ATP (a reaction with a free-energy change $\Delta\mu_{\mathrm{ATP}} \approx 15$–$30 k_B T$ [61]) for every forward step ($d \approx 8$ nm). At 298 K, $1 k_B T = 4.114$ pN nm, resulting in a chemical driving force $f_{\mathrm{chem}} = \Delta\mu_{\mathrm{ATP}}/d \approx$ 8–15 pN, in line with our previous estimate.

We estimate the motor diffusivity using $\mathrm{v}_{\mathrm{max}} = \beta f_s D_m$. For kinesin-1 the maximum velocity is $\mathrm{v}_{\mathrm{max}} \approx 1$–$2$ μm s^{-1} and the stall force is $f_s \approx$ 6–8 pN [8], while for myosin V, $v_{\mathrm{max}} \approx 8$ nm s^{-1} [7] and $f_s \approx$ 10–15 pN [16]. This suggests that in both cases $D_m = \mathcal{O}(10^{-3})$ μm^2 s^{-1}. Alternatively, using experimental estimates of rate constants for forward and reverse steps yields an estimate for kinesin-1 motor diffusivity of $D_m \approx 4 \times 10^{-3}$ μm^2 s^{-1} [62].

Cargo diffusivity can vary by orders of magnitude depending on the type of molecular cargo. As one example, diffusivity of vesicles (with radii on the order of 300 nm) in neurons is estimated to be of order 10^{-3} μm^2 s^{-1} [63]. Other measurements of vesicles and vesicle-sized beads in cytoplasm have found diffusivities on the order of 10^{-4}–10^{-2} μm^2 s^{-1} [64]. Larger cargo such as organelles, for example mitochondria which have diameters as large as 2 μm, will have even smaller diffusivities. Thus for intracellular transport of vesicles and organelles we expect $D_c/D_m \in [10^{-3}, 1]$.

We use these parameter ranges to estimate the relaxation time $\tau_{\mathrm{relax}} = [\beta\kappa(D_m + ND_c)]^{-1}$ in section 3.1. Based on the ranges and estimates above, we get a maximum value of about 0.02 s (taking $\kappa = 0.2$ pN nm^{-1}, $T = 298$ K, $D_m = 10^{-3}$ μm^2 s^{-1}, $D_c = 10^{-4}$ μm^2 s^{-1}, and $N = 1$). Using more typical values of these parameters (for example $\kappa = 0.5$ pN nm^{-1}, $D_m = 4 \times 10^{-3}$ μm^2 s^{-1}, $D_c = 10^{-3}$ μm^2 s^{-1}, and $N = 10$) gives a much smaller estimate $\tau_{\mathrm{relax}} \approx 5 \times 10^{-4}$ s.

Appendix C. Stochasticity metrics

Figure C1 shows the N-dependence of the three stochasticity metrics we introduced in section 3.2.1: the effective diffusivity D_{eff} (equation (11)), the coefficient of variation θ (equation (12)), and the Fano factor ϕ (equation (13)).

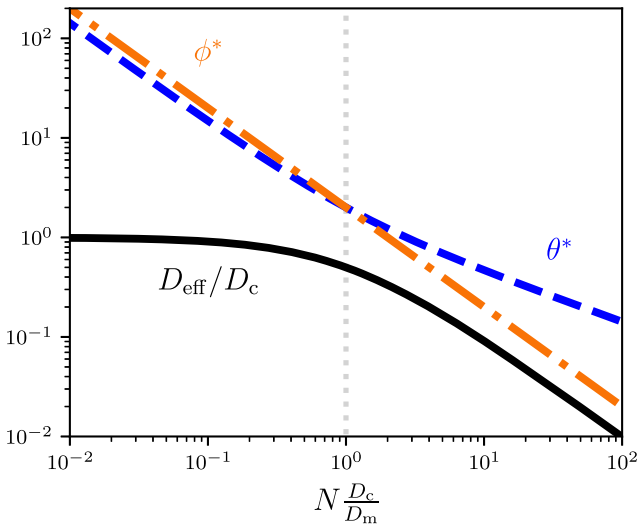

Figure C1. N-dependence of the performance metrics used to quantify stochasticity: the effective diffusivity $D_{\mathrm{eff}}/D_{\mathrm{c}}$, the coefficient of variation $\theta^* = \theta\beta f_{\mathrm{chem}}\sqrt{t/D_{\mathrm{c}}}$, and the Fano factor $\phi^* = \beta f_{\mathrm{chem}}(D_{\mathrm{m}}/D_{\mathrm{c}})\phi$; all in dimensionless units.

Appendix D. Simulations for motors with significant energy barriers

We add to each motor a periodic potential-energy landscape of the form $V(x_i) = E^{\ddagger}\cos\left(x_i/\ell\right)$, where $2E^{\ddagger}$ is the height of the energy barriers between successive meta-stable states (local energy minima), and $2\pi\ell$ is the period. Each motor's dynamics satisfy

$$\dot{x}_i = \beta D_{\mathrm{m}}\left[f_{\mathrm{chem}} - \kappa(x_i - x_{\mathrm{c}}) - f_{\mathrm{max}}\,\sin(x_i/\ell)\right] + \eta_i, \tag{D1}$$

where $f_{\mathrm{max}} = E^{\ddagger}/\ell$ is the maximum conservative force arising from the periodic potential. (The cargo motion still obeys equation (1a).) While these new equations of motion cannot be solved analytically, we can numerically simulate the dynamics of this system, by integrating the $N+1$ Langevin equations for a given value of N. Obtaining full time-dependent probability distributions through simulation is computationally intractable for large N, so we compute only properties that depend solely on the average system dynamics.

Figures D1(a)–(c) shows how three important performance metrics, the mean velocity $\langle v\rangle$, the Stokes efficiency η_{S}, and the chemical power consumption P_{chem}, scale with the number N of motors, for varying ratios $f_{\mathrm{max}}/f_{\mathrm{chem}}$ between the maximum conservative force and the chemical driving force on each motor. In the limit as $f_{\mathrm{max}}/f_{\mathrm{chem}} \to 0$, this system is identical to the analytically tractable system (described by equation (1)) that we have focused on in this paper. In the large- and small-N regimes, the scaling of the three performance metrics with N is consistent with the scaling laws from table 1, shown in black dashed and dotted lines.

Appendix E. Motor binding/unbinding

As discussed in section 4, we investigate the effects of dynamically changing motor number using a simple stochastic model for motor binding/unbinding based on [21]. The motor number N undergoes a random walk, with rates

$$N \to N+1\colon\ k_N^+ = k_0^+(N_{\mathrm{max}} - N), \tag{E1a}$$

$$N \to N-1\colon\ k_N^- = k_0^- N. \tag{E1b}$$

Here k_0^+ and k_0^- are base rates of binding and unbinding, and N_{max} is the maximum number of motors that can bind a given cargo. The distribution $P(N)$ satisfies the master equation

$$\frac{\partial}{\partial t}P(N) = k_{N+1}^- P(N+1) + k_{N-1}^+ P(N-1) - (k_N^+ + k_N^-)P(N), \tag{E2}$$

with reflecting boundaries at $N = 1$ and $N = N_{\mathrm{max}}$. (We set a reflecting boundary at $N = 1$ rather than $N = 0$ because we are interested only in the behavior of the system when there are motors attached.)

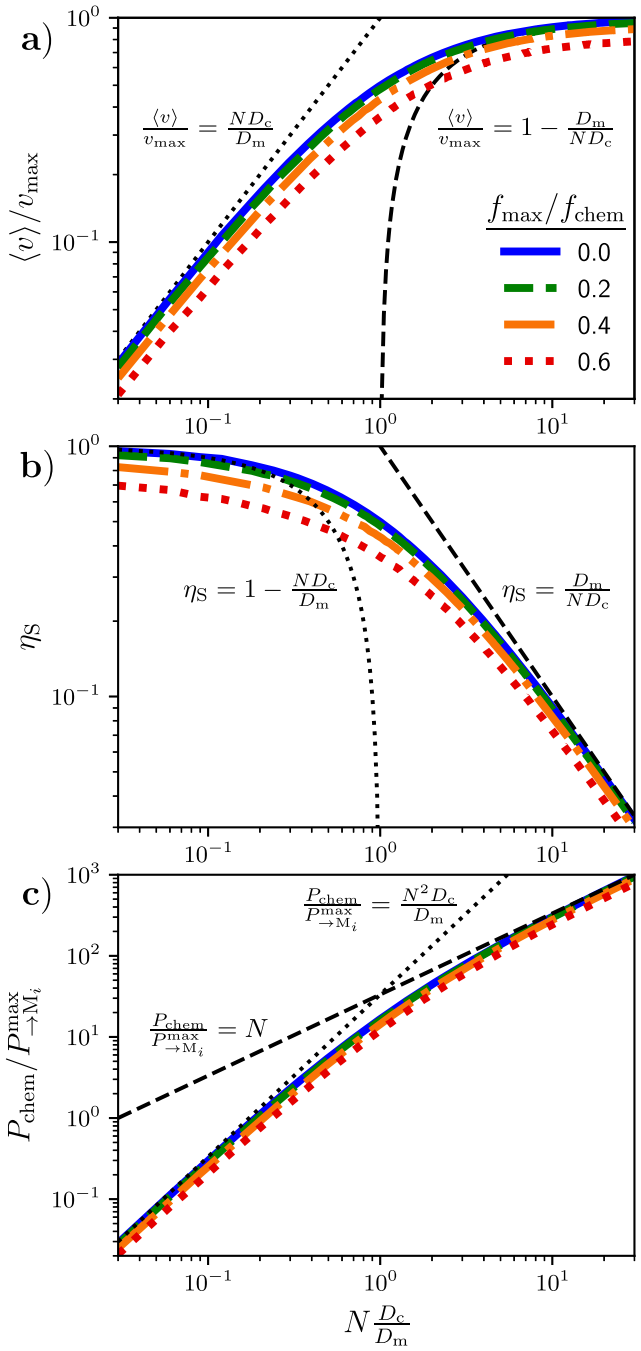

Figure D1. Scaling of the scaled mean velocity $\langle v\rangle/v_{\max}$, the Stokes efficiency η_S, and the scaled chemical power consumption $P_{\chem}/P^{\max}_{\to M_i}$, as a function of the motor number N scaled by the diffusivity ratio D_m/D_c. We simulate $N \in [1, 2, 3, \ldots, 1000]$ for several different ratios $f_{\max}/f_{\chem}$ of the maximum conservative force to the chemical driving force. For $f_{\max}/f_{\chem} = 0$ (solid blue) we recover our analytically tractable model. Black curves indicate the scaling laws from table 1 in the small-N (dotted) and large-N (dashed) limits. Parameters: $f_{\chem} = 10$, $\kappa = 1$, $D_c = 0.03D_m$; in dimensionless units chosen so that $D_m = \kappa = \ell = 1$.

The master equation (E2) with these boundary conditions has a time-independent steady-state solution. To simplify the analysis we take the limit $N_{\max} \to \infty$ and $k_0^+ \to 0$ such that $N_{\max}\, k_0^+/k_0^- = \lambda$ is fixed. The steady-state solution is then

$$P(N) = \frac{\lambda^N}{N!(e^\lambda - 1)}, \tag{E3}$$

defined for $N \geqslant 1$. This is a zero-truncated Poisson distribution [65], with mean

$$\langle N\rangle = \frac{\lambda}{1 - e^{-\lambda}}. \tag{E4}$$

We can then use this distribution to calculate mean values of different steady-state properties of the transport system, averaged over $P(N)$. In particular, we estimate the error involved in assuming the system

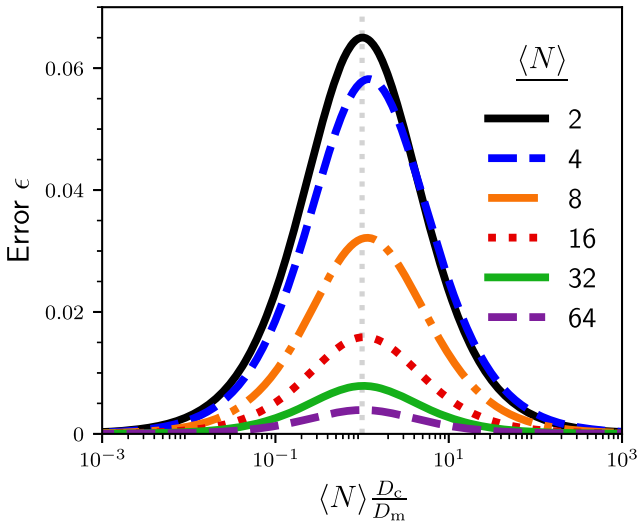

Figure E1. Error (E5) in mean velocity between fluctuating (described by equation (E3)) and constant motor number, both with equal mean motor number $\langle N \rangle$, as a function of $\langle N \rangle D_c/D_m$. Vertical gray dotted line indicates $\langle N \rangle D_c/D_m = 1$.

is well described by a constant (rather than fluctuating) number of motors. We use the mean velocity as an example.

For a given average number $\langle N \rangle$ of motors, we compare the mean velocity (10) evaluated at fixed $N = \langle N \rangle$ to the velocity instead averaged over the distribution $P(N)$ with the parameter λ chosen so that $\sum_{N=1}^{\infty} NP(N) = \langle N \rangle$. The error in mean velocity incurred by assuming fixed N is

$$\epsilon \equiv \frac{\left\langle v\left(\langle N \rangle_{P(N)}\right)\right\rangle_{\mathrm{ss}} - \left\langle \langle v(N) \rangle_{\mathrm{ss}} \right\rangle_{P(N)}}{\left\langle \langle v(N) \rangle_{\mathrm{ss}} \right\rangle_{P(N)}}, \tag{E5}$$

where $\langle \cdot \rangle_{\mathrm{ss}}$ denotes an ensemble average over the system dynamics at fixed N, and $\langle \cdot \rangle_{P(N)}$ denotes an average over the probability distribution $P(N)$.

Figure E1 shows this error over a range of different values of $\langle N \rangle$ and D_c/D_m. The error resulting from assuming a fixed number of motors is less than 7%, and we find similar magnitudes of error for other quantities. Note that the error is maximized for small $\langle N \rangle$, and for $\langle N \rangle D_c/D_m \approx 1$.

ORCID iDs

Matthew P Leighton https://orcid.org/0000-0002-4765-9967
David A Sivak https://orcid.org/0000-0003-4815-4722

References

[1] Schrôdinger E 1944 *What is Life?* (Cambridge: Cambridge University Press)
[2] Mogre S, Brown A I and Koslover E F 2020 Getting around the cell: physical transport in the intracellular world *Phys. Biol.* **17** 061003
[3] Purcell E M 1977 Life at low Reynolds number *Am. J. Phys.* **45** 3
[4] Hancock W O 2008 Intracellular transport: kinesins working together *Curr. Biol.* **18** R715
[5] Brown A I and Sivak D A 2019 Theory of nonequilibrium free energy transduction by molecular machines *Chem. Rev.* **120** 434
[6] Seifert U 2012 Stochastic thermodynamics, fluctuation theorems and molecular machines *Rep. Prog. Phys.* **75** 126001
[7] Purcell T J *et al* 2011 Nucleotide pocket thermodynamics measured by EPR reveal how energy partitioning relates myosin speed to efficiency *J. Mol. Biol.* **407** 79
[8] Fallesen T L, Macosko J C and Holzwarth G 2011 Force-velocity relationship for multiple kinesin motors pulling a magnetic bead *Eur. Biophys. J.* **40** 1071
[9] Encalada S E, Szpankowski L, Xia C-H and Goldstein L S B 2011 Stable kinesin and dynein assemblies drive the axonal transport of mammalian prion protein vesicles *Cell* **144** 551
[10] Cooke R 1997 Actomyosin interaction in striated muscle *Physiol. Rev.* **77** 671
[11] Leopold P L, McDowall A W, Pfister K K, Bloom G S and Brady S T 1992 Association of kinesin with characterized membrane-bounded organelles *Cell Motil. Cytoskeleton* **23** 19
[12] Hatsumi M and Endow S A 1992 Mutants of the microtubule motor protein, nonclaret disjunctional, affect spindle structure and chromosome movement in meiosis and mitosis *J. Cell Sci.* **101** 547

[13] Shtridelman Y, Cahyuti T, Townsend B, DeWitt D and Macosko J C 2008 Force–velocity curves of motor proteins cooperating *in vivo Cell Biochem. Biophys.* **52** 19
[14] Shtridelman Y, Holzwarth G M, Bauer C T, Gassman N R, DeWitt D A and Macosko J C 2009 *In vivo* multimotor force–velocity curves by tracking and sizing sub-diffraction limited vesicles *Cel. Mol. Bioeng.* **2** 190
[15] Svoboda K and Block S M 1994 Force and velocity measured for single kinesin molecules *Cell* **77** 773
[16] Rastogi K, Puliyakodan M S, Pandey V, Nath S and Elangovan R 2016 Maximum limit to the number of myosin ii motors participating in processive sliding of actin *Sci. Rep.* **6** 1
[17] DelRosso N V and Derr N D 2017 Exploiting molecular motors as nanomachines: the mechanisms of de novo and re-engineered cytoskeletal motors *Curr. Opin. Biotechnol.* **46** 20
[18] Furuta K, Furuta A, Toyoshima Y Y, Amino M, Oiwa K and Kojima H 2013 Measuring collective transport by defined numbers of processive and nonprocessive kinesin motors *Proc. Natl Acad. Sci.* **110** 501
[19] Derr N D, Goodman B S, Jungmann R, Leschziner A E, Shih W M and Reck-Peterson S L 2012 Tug-of-war in motor protein ensembles revealed with a programmable dna origami scaffold *Science* **338** 662
[20] Hunt A J, Gittes F and Howard J 1994 The force exerted by a single kinesin molecule against a viscous load *Biophys. J.* **67** 766
[21] Klumpp S and Lipowsky R 2005 Cooperative cargo transport by several molecular motors *Proc. Natl Acad. Sci.* **102** 17284
[22] Kunwar A and Mogilner A 2010 Robust transport by multiple motors with nonlinear force–velocity relations and stochastic load sharing *Phys. Biol.* **7** 016012
[23] Zimmermann E and Seifert U 2015 Effective rates from thermodynamically consistent coarse-graining of models for molecular motors with probe particles *Phys. Rev.* E **91** 022709
[24] Brown A I and Sivak D A 2019 Pulling cargo increases the precision of molecular motor progress *Europhys. Lett.* **126** 40004
[25] Korn C B, Klumpp S, Lipowsky R and Schwarz U S 2009 Stochastic simulations of cargo transport by processive molecular motors *J. Chem. Phys.* **131** 12B624
[26] McKinley S A, Athreya A, Fricks J and Kramer P R 2012 Asymptotic analysis of microtubule-based transport by multiple identical molecular motors *J. Theor. Biol.* **305** 54
[27] Li X, Lipowsky R and Kierfeld J 2012 Critical motor number for fractional steps of cytoskeletal filaments in gliding assays *PLoS One* **7** e43219
[28] Bhat D and Gopalakrishnan M 2016 Transport of organelles by elastically coupled motor proteins *Eur. Phys. J.* E **39** 1
[29] Bhat D and Gopalakrishnan M 2017 Stall force of a cargo driven by *N* interacting motor proteins *Europhys. Lett.* **117** 28004
[30] Arpağ G, Shastry S, Hancock W O and Tüzel E 2014 Transport by populations of fast and slow kinesins uncovers novel family-dependent motor characteristics important for *in vivo* function *Biophys. J.* **107** 1896–1904
[31] Kawaguchi K, Uemura S and Ishiwata S I 2003 Equilibrium and transition between single- and double-headed binding of kinesin as revealed by single-molecule mechanics *Biophys. J.* **84** 1103
[32] Schnitzer M J and Block S M 1997 Kinesin hydrolyses one ATP per 8 nm step *Nature* **388** 386
[33] Visscher K, Schnitzer M J and Block S M 1999 Single kinesin molecules studied with a molecular force clamp *Nature* **400** 184
[34] Horowitz J M 2015 Multipartite information flow for multiple maxwell demons *J. Stat. Mech.* P03006
[35] Risken H 1996 Fokker–Planck equation *The Fokker-Planck Equation* (Berlin: Springer) pp 63–95
[36] Toprak E, Yildiz A, Hoffman M T, Rosenfeld S S and Selvin P R 2009 Why kinesin is so processive *Proc. Natl Acad. Sci.* **106** 12717
[37] Nakul U and Gopalakrishnan M 2021 Frictional drag produced by motor proteins during cargo transport *Europhys. Lett.* **133** 68002
[38] Leibler S and Huse D A 1993 Porters versus rowers: a unified stochastic model of motor proteins *J. Cell Biol.* **121** 1357
[39] Brown C E 1998 Coefficient of variation *Applied Multivariate Statistics in Geohydrology and Related Sciences* (Berlin: Springer) pp 155–7
[40] de Groot S and Mazur P 1969 *Non-equilibrium Thermodynamics* (Amsterdam: North-Holland)
[41] Wang H and Oster G 2002 The Stokes efficiency for molecular motors and its applications *Europhys. Lett.* **57** 134
[42] Pietzonka P, Barato A C and Seifert U 2016 Universal bound on the efficiency of molecular motors *J. Stat. Mech.* 124004
[43] Lathouwers E, Lucero J N and Sivak D A 2020 Nonequilibrium energy transduction in stochastic strongly coupled rotary motors *J. Phys. Chem. Lett.* **11** 5273–8
[44] Wagoner J A and Dill K A 2019 Opposing pressures of speed and efficiency guide the evolution of molecular machines *Mol. Biol. Evol.* **36** 2813
[45] Wagoner J A and Dill K A 2021 Evolution of mechanical cooperativity among myosin II motors *Proc. Natl Acad. Sci.* **118** 20
[46] Horowitz J M and Gingrich T R 2020 Thermodynamic uncertainty relations constrain non-equilibrium fluctuations *Nat. Phys.* **16** 15
[47] Barato A C and Seifert U 2015 Thermodynamic uncertainty relation for biomolecular processes *Phys. Rev. Lett.* **114** 158101
[48] Saryal S, Friedman H M, Segal D and Agarwalla B K 2019 Thermodynamic uncertainty relation in thermal transport *Phys. Rev.* E **100** 042101
[49] Shoval O, Sheftel H, Shinar G, Hart Y, Ramote O, Mayo A, Dekel E, Kavanagh K and Alon U 2012 Evolutionary trade-offs, pareto optimality, and the geometry of phenotype space *Science* **336** 1157
[50] Gagliano J, Walb M, Blaker B, Macosko J C and Holzwarth G 2010 Kinesin velocity increases with the number of motors pulling against viscoelastic drag *Eur. Biophys. J.* **39** 801
[51] Kaneko T, Ando S, Furuta K Y, Oiwa K, Shintaku H, Kotera H and Yokokawa R 2019 Transport of microtubules according to the number and spacing of kinesin motors on gold nano-pillars *Nanoscale* **11** 9879
[52] Howard J, Hudspeth A J and Vale R D 1989 Movement of microtubules by single kinesin molecules *Nature* **342** 154
[53] Svoboda K, Schmidt C F, Schnapp B J and Block S M 1993 Direct observation of kinesin stepping by optical trapping interferometry *Nature* **365** 721
[54] Wijeratne S, Fiorenza S A, Subramanian R and Betterton M 2020 Motor guidance by long-range communication through the microtubule highway (bioRxiv Preprint) 2020.12.23.424221
[55] Klumpp S, Nieuwenhuizen T M and Lipowsky R 2005 Movements of molecular motors: ratchets, random walks and traffic phenomena *Physica* E **29** 380
[56] Carter N J and Cross R A 2005 Mechanics of the kinesin step *Nature* **435** 308
[57] Ndlec F J, Surrey T, Maggs A C and Leibler S 1997 Self-organization of microtubules and motors *Nature* **389** 305
[58] Kumar J, Yu H and Sheetz M P 1995 Kinectin, an essential anchor for kinesin-driven vesicle motility *Science* **267** 1834
[59] Veigel C, Schmitz S, Wang F and Sellers J R 2005 Load-dependent kinetics of myosin-V can explain its high processivity *Nat. Cell Biol.* **7** 861

[60] Debold E P, Patlak J B and Warshaw D M 2005 Slip sliding away: load-dependence of velocity generated by skeletal muscle myosin molecules in the laser trap *Biophys. J.* **89** L34
[61] Milo R and Phillips R 2015 *Cell Biology by the Numbers* (New York: Garland Science)
[62] Vu H T, Chakrabarti S, Hinczewski M and Thirumalai D 2016 Discrete step sizes of molecular motors lead to bimodal non-Gaussian velocity distributions under force *Phys. Rev. Lett.* **117** 078101
[63] Ahmed W W and Saif T A 2014 Active transport of vesicles in neurons is modulated by mechanical tension *Sci. Rep.* **4** 1
[64] Luby-Phelps K 1999 Cytoarchitecture and physical properties of cytoplasm: volume, viscosity, diffusion, intracellular surface area *Int. Rev. Cytology* **192** 189
[65] Johnson N L, Kemp A W and Kotz S 2005 *Univariate Discrete Distributions* vol 444 (New York: Wiley)